J Appl Electrochem (2014) 44:1185–1191
DOI 10.1007/s10800-014-0744-5

RESEARCH ARTICLE

Facile synthesis of NiO/MWCNT composites by a vacuum solution infiltration method for lithium-ion batteries

Yanhong Yin · Yujie Jia · Xiaoting Zhang · Chao Ma · Zhixian Sun · Shuting Yang

Received: 27 June 2014 / Accepted: 3 September 2014 / Published online: 10 September 2014

Abstract Nickel oxide/multi-walled carbon nanotube (NiO/MWCNT) composites were fabricated via a vacuum solution infiltration method combined with a calcination treatment. The crystalline structure and morphology were characterized by X-ray diffraction (XRD), scanning electron microscopy (SEM), and transmission electron microscopy (TEM) with selected area electron diffraction (SAED). The specific surface area, pore size, and pore volume were obtained by Brunauer–Emmett–Teller (BET). The as-prepared NiO/MWCNT composites deliver an initial discharge capacity of 1,015 mAh g^{-1} with 86 % capacity retention (873 mAh g^{-1}) after 50 cycles at a current rate of 0.1 C. The enhanced electrochemical performance is ascribed to the nanosized NiO and MWCNTs which can act as buffering matrix to relax the volume expansion and electron transfer conductor in the composites.

Keywords Nickeloxide/multi-walled nanotube composites · Charge/discharge and cycling performance · Vacuum solution infiltration process · Anode material · Lithium-ion batteries

Y. Yin · Y. Jia · X. Zhang · C. Ma · Z. Sun · S. Yang (✉)
School of Chemistry and Chemical Engineering, Henan Normal University, Xinxiang 453007, Henan, China
e-mail: shutingyang@foxmail.com

Y. Yin · Y. Jia · X. Zhang · C. Ma · Z. Sun · S. Yang
Engineering Technology Research Center of Motive Power and Key Materials of Henan Province, Xinxiang 453007, Henan, China

Y. Yin · Y. Jia · X. Zhang · C. Ma · Z. Sun · S. Yang
Collaborative Innovation Center of Henan Province for Motive Power and Key Materials, Henan Normal University, Xinxiang 453007, Henan, China

1 Introduction

Lithium-ion batteries (LIBs) are the most feasible candidate in energy storage and conversion due to their high power and energy density [1–3]. Many researchers have developed novel electrode materials and facile approaches for the next generation LIBs. Recently, transition metal oxides (such as CuO, Fe_2O_3, MnO_2, MnO, and NiO) have been intensively investigated as alternative anode materials due to their excellent theoretical capacity (500–1,000 mAh g^{-1}) [4–6]. Among these anode materials, NiO has attracted significant attentions due to its outstanding theoretical capacity of 718 mAh g^{-1}, low cost, environmental friendliness, and accessible preparation [7]. To date, numerous NiO nanostructures, such as nanospheres [8], nanofibers [9], nanosheets [10], nanocapsules [11], and nanoplates [12], have been investigated. Nonetheless, NiO anode material with poor conductivity exhibits a poor cycling performance and rate capability because its drastic volume expansion will lead to the pulverization and exfoliation during the discharge/charge process.

Coating the oxides with carbon or forming composites with carbon materials such as nano carbon, graphene, carbon nanotubes, and so on is an effective way to resolve this problem [13–15]. On one hand, carbon materials can act as a barrier to suppress the aggregation of active particles, and thus increase their structural stability during cycling. On the other hand, they can also act as a buffering matrix to accommodate the volume expansion during the Li^+ insertion/extraction processes. Multi-walled carbon nanotubes (MWCNTs) with high electrical conductivity and structure adaptability can act as a buffer matrix and an electron transfer medium [16]. Numerous strategies have been developed to synthesize NiO/MWCNT composites such as thermal decomposition process [17], co-

precipitation process [18], electrochemical process [19], and electrospinning process [20]. However, most of these methods are complex and difficult to scale up. At present, the mass production of NiO/MWCNT composites with excellent electrochemical performance has not been reported.

Vacuum solution infiltration method would be a good choice as this method can take the metal salt solution to the porous carbon materials under vacuum and assure the sufficient impregnation, which has been used in the preparation of SnO_2/CNTs [21]. However, only a few reports on the synthesis of NiO/MWCNT composites via this method have been found. Herein, we describe the synthesis of NiO/MWCNT composites via a vacuum solution infiltration technique. Meanwhile, its morphology, structure, and electrochemical performance of the NiO/MWCNT composites were characterized. The resultant composites exhibited greatly improved electrochemical performance with high specific capacity as anode material for LIBs, demonstrating that the synthesized composite is a promising candidate of anode material for LIBs.

2 Experimental

2.1 Materials

$Ni(NO_3)_2{\cdot}6H_2O$ and MWCNTs were purchased from Tianjin Hongyan Chemical Reagent Factory and Chengdu Organic Chemicals Co. Ltd, Chinese Academy of Sciences, respectively. All the other reagents were of analytical grade and used as received without further purification.

2.2 Synthesis of NiO/MWCNT composites

MWCNTs, which dried at 120 °C in vacuum for 12 h, were added to a single-necked bottle. The weight ratio of MWCNTs to the final product NiO calcined from $Ni(NO_3)_2{\cdot}6H_2O$ is 1:2. Subsequently, the solution was heated to 60 °C and kept in vacuum condition for 20 min under constant magnetic stirring. A certain amount of $Ni(NO_3)_2{\cdot}6H_2O$ was added in distilled water under vigorous stirring to form a homogenous saturated aqueous solution. Then $Ni(NO_3)_2$ aqueous solution was added into vacuumed bottle, which will be absorbed by the MWCNTs immediately. After then, the above suspension was put into an open glass beaker to evaporate the distilled water at 60 °C for 12 h. Finally, the NiO/MWCNT composites were obtained after heat treatment at 350 °C for 2 h in a high purity nitrogen atmosphere. For comparison, pure NiO was prepared by directly evaporating the $Ni(NO_3)_2{\cdot}6H_2O$ solution with a following calcination process.

2.3 Material characterization

Crystal structure of the products was characterized by X-ray diffraction (XRD, Bruker AXS D8) with Cu Kα radiation. Thermogravimetric (TG) analysis of the NiO/MWCNT composites was investigated by thermal analysis apparatus (TG, STA449C, German Netzsch). The morphology was examined by a scanning electron microscope (SEM, SU-8010, HITACHI) and transmission electron microscope (TEM, JEM-2100, JEOL) with a selected area electron diffraction (SAED). The specific surface area and porosity analysis of the composites were measured by the standard Brunauer–Emmett–Teller method (BET) using a Tristar 3020 surface area and pore size analyzer.

2.4 Electrochemical measurements

The electrochemical performance was evaluated using CR2016 coin cells. The working electrode was prepared by casting slurries consisting of the as-prepared powder, Super P carbon black, and polyvinylidene fluoride (PVDF) in a weight ratio of 80:10:10 on a copper foil with *N*-methyl-2-pyrrolidine (NMP) as solvent. Subsequently, the electrode was dried at 80 °C for 12 h in the vacuum. The amount of active materials (NiO) was controlled as the same either in the NiO/MWCNTs electrode or in the NiO electrode. The separator was a polypropylene membrane (Celgard 2400). Lithium metal was used as counter and reference electrode. The electrolyte was 1 M $LiPF_6$ in a mixture of ethylene carbonate (EC) and diethyl carbonate (DEC) (1:1 volume). Galvanostatic charge–discharge experiment was conducted using LAND Cell test system (CT2001A, Wuhan) in the voltage range of 0.01–3.0 V (vs. Li/Li^+). Cyclic voltammetry was performed on a CHI660D electrochemical workstation at a scan rate of 0.1 mV s^{-1}.

3 Results and discussion

3.1 Crystal structure of the pure NiO and NiO/MWCNT composites

Figure 1 illustrates the XRD patterns of both pure NiO and NiO/MWCNT composites. The broad hump at ~25° marked with asterisk corresponds to the turbostratic structure of MWCNTs in the composites [22]. All the other diffraction peaks at 37.25°, 43.28°, 62.88°, 75.41°, and 79.41° can be indexed to (111), (200), (220), (311), and (222) crystal planes of NiO (JCPDS 47-1049). The XRD pattern of NiO/MWCNT composites shows broader and weaker reflections compared with pure NiO, which can be attributed to the dispersion of NiO nanoparticles in the surface of MWCNTs. Herein, the MWCNTs as a buffering matrix can prevent the growing of crystals during the

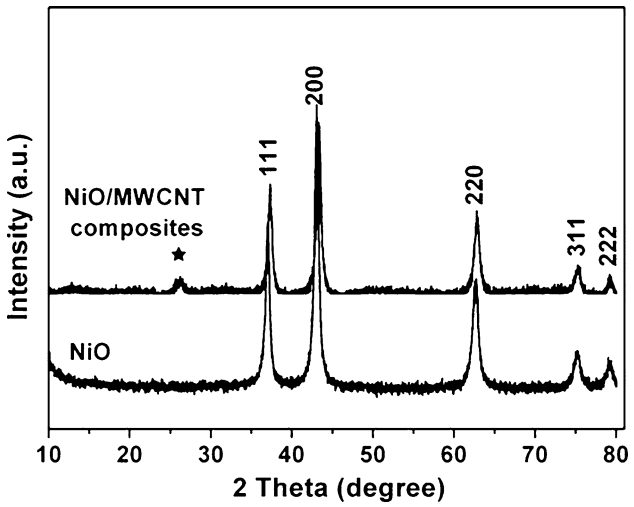

Fig. 1 XRD patterns of pure NiO and the NiO/MWCNT composites

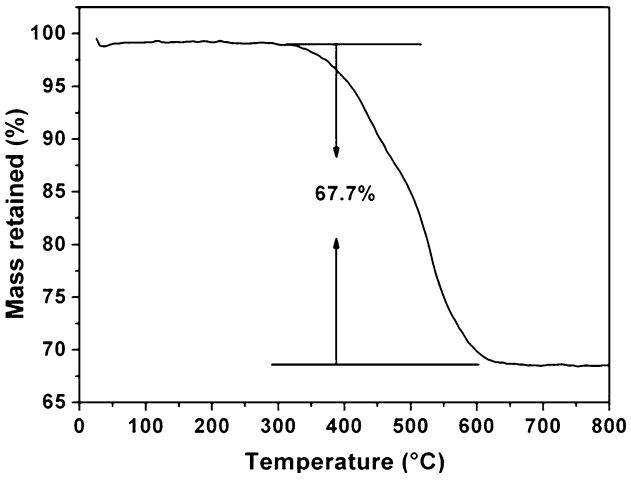

Fig. 2 TG curve of the NiO/MWCNT composites in air atmosphere

calcination process. According to the Scherrer formula, the particle size of NiO in the composites is estimated to be ~12 nm which is smaller than that of pure NiO (15 nm).

3.2 TG analysis of the NiO/MWCNT composites

TG was used to determine the content of MWCNTs in the NiO/MWCNT composites in air atmosphere at a heating rate of 10 °C min^{-1}, as shown in Fig. 2. The TG curve shows that the composite has a weight loss of 0.78 % between 30 and 200 °C, which can be attributed to evaporation of the adsorbed water in the composites. A large weight loss occurs from 350 to 600 °C, corresponding to the oxidation decomposition of carbon nanotubes. There is no more weight loss above 600 °C. Therefore, the mass percentage of NiO in the NiO/MWCNT composites is about 67.7 %, which is very close to the pre-set value.

3.3 Morphology of the NiO/MWCNT composites

The detailed morphological and structural features of the composites are shown in Fig. 3. Figure 3a shows the SEM and TEM images of pristine MWCNTs with a diameter of 30–50 nm. The SEM image of NiO/MWCNT composites shown in Fig. 3b keeps the overall morphology of MWCNTs. The diameter of the composites is a little larger than that of MWCNTs, indicating that NiO particles have deposited on the surface of MWCNTs. Meanwhile, there are no obvious NiO particles in the SEM image, demonstrating that the NiO particles are uniform distribution. Figure 3c shows the TEM image of the NiO/MWCNT composites. It can be seen that NiO nanoparticles with a particle size of about 12 nm randomly disperse on the MWCNTs. The inset in Fig. 3c is a selected area electron diffraction (SAED) pattern taken from the edge of the composites. The bright diffraction rings made of discrete spots indicate the polycrystalline structure of the product. Figure 3e and f show the high resolution TEM (HRTEM) images of the square area in Fig. 3d. The lattice fringe with an interplanar distance of 0.35 nm can be attributed to the (002) plane of MWCNTs. While the lattice fringes of ~0.21 nm agrees well with the (200) planes of NiO (Fig. 3f), illustrating the formation of crystalline NiO nanoparticles on MWCNTs. Morphology of NiO/MWCNT composites after 50 cycles is shown in Fig. 3g. After being cycled, texture structures of the NiO/MWCNT composites disappeared. The particles are connected to each other tightly, showing a relatively smooth surface, which may be due to the binding agent used during the electrode preparation process, or the formation of SEI membrane during charge–discharge process. Similar structure and morphology variations are reported in literature [23].

3.4 Surface structure characteristics of pure MWCNTs and NiO/MWCNT composites

Nitrogen adsorption–desorption isotherms of pure MWCNTs and NiO/MWCNT composites are shown in Fig. 4a, and the corresponding parameters are presented in Table 1. Both of the samples show typical type-IV curves, with hysteresis loops at a relative pressure of 0.5–1.0 P/P_0, indicating the porous structure of the materials. The hysteresis loop at medium relative pressure in the adsorption–desorption isotherm illustrates the presence of mesoporosity, while the rise after $P/P_0 > 0.9$ represents of macroporosity contributed by the interspaces between MWCNTs. However, the NiO/MWCNT composites have a relatively smaller BET surface area, pore size, and pore volume than that of pure MWCNTs, illustrating the formation of NiO particles on or among the gaps of the carbon nanotubes. The pore size distributions of pure

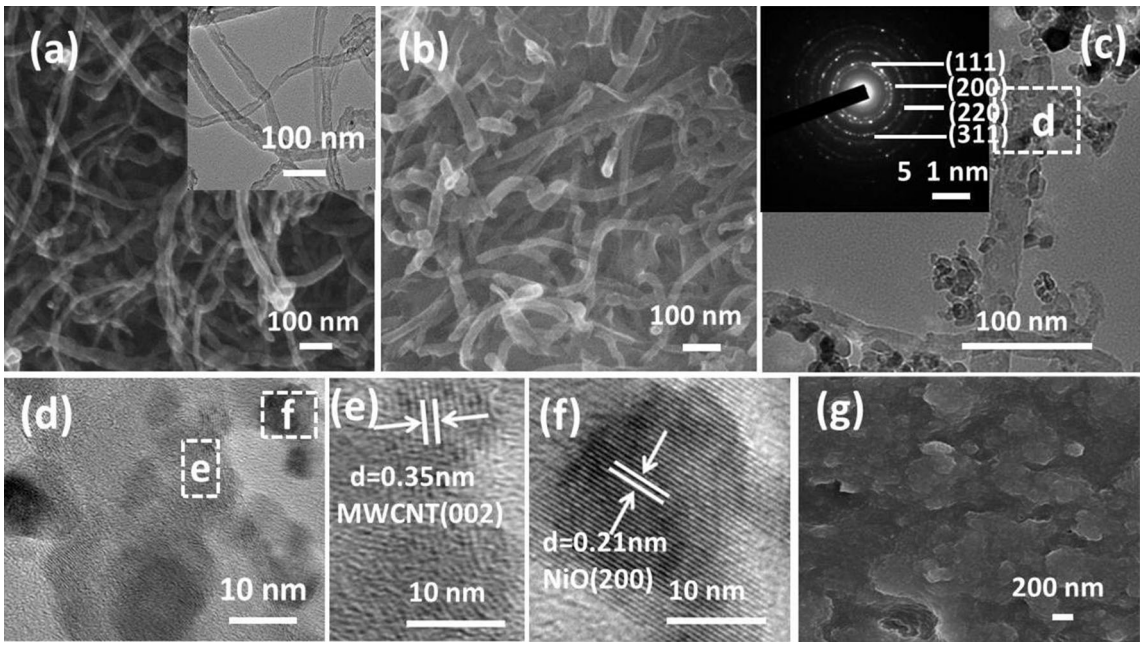

Fig. 3 SEM and TEM micrographs of MWCNTs (**a**), SEM micrograph (**b**), TEM image (**c**), and *inset* shows selected area electronic diffraction (SAED) pattern, HRTEM image (**d**–**f**), and SEM images after 50 cyclings (**g**) of the NiO/MWCNT composites

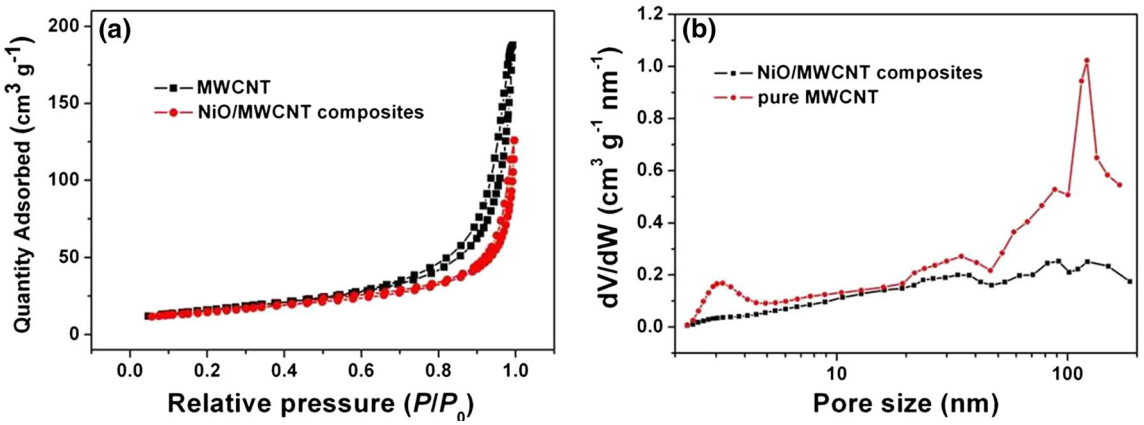

Fig. 4 Nitrogen adsorption–desorption isotherms at 77 K of the pure MWCNTs and NiO/MWCNT composites (**a**) and their pore size distributions (**b**)

Table 1 BET results for the pure MWCNTs and the NiO/MWCNT composites

Samples	Surface area ($m^2\ g^{-1}$)	Pore size (nm)	Pore volume ($cm^3\ g^{-1}$)
MWCNTs	115	190	0.55
The NiO/MWCNT composites	109	149	0.41

MWCNT and NiO/MWCNT composites calculated by Barrett–Joyner–Halenda (BJH) method are shown in Fig. 4b; it can be seen that both of the samples mainly have two kinds of pore size distribution: one is 20–50 nm (mesopores), the other is >50 nm (macropores). But it is obvious that the NiO/MWCNT composites have a smaller pore size than that of pure MWCNT, indicating that some of the pores within the MWCNT are occupied by NiO nanoparticles.

3.5 Electrochemical performance of the pure NiO and NiO/MWCNT composites

The galvanostatic charge–discharge curves and the cycling performance of the pure NiO and NiO/MWCNT composites at the current density of 0.1 C are illustrated in Fig. 5. Figure 5a and b show charge–discharge curves of NiO and

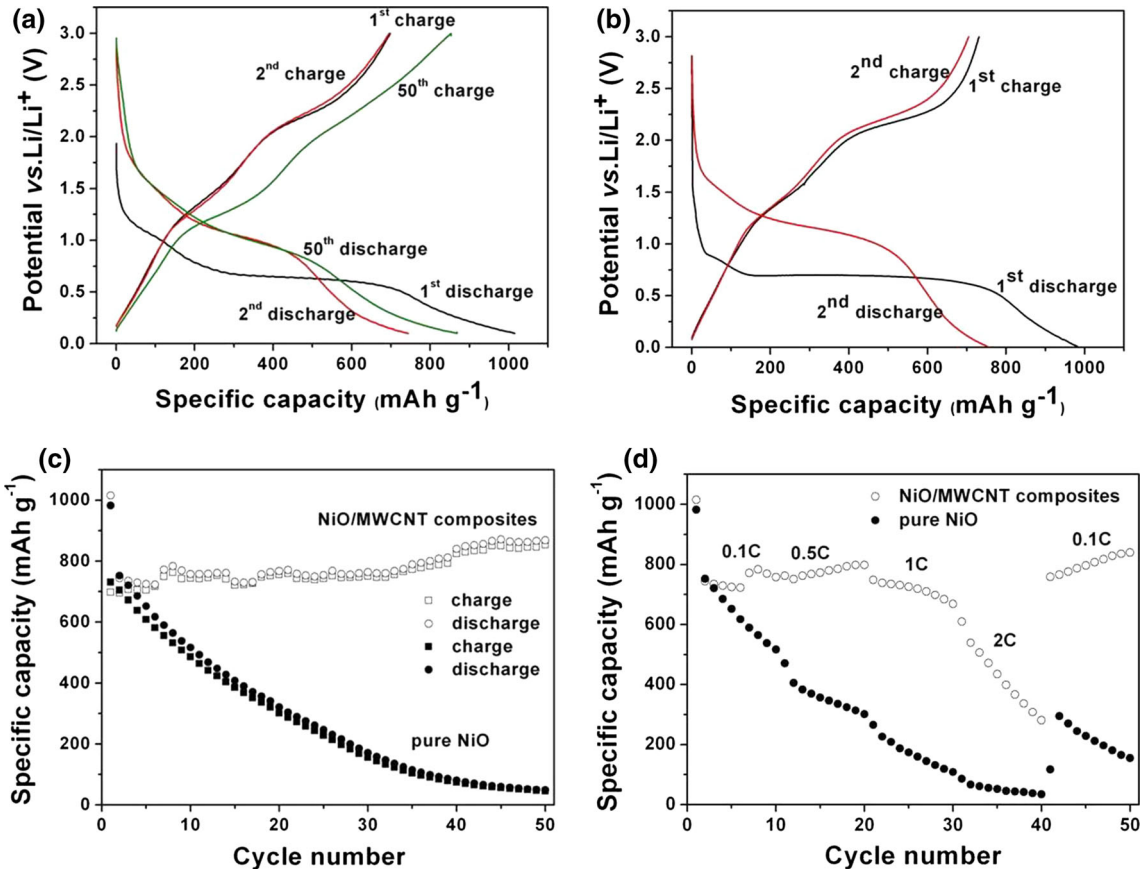

Fig. 5 Charge–discharge voltage profiles of the NiO/MWCNT composites (**a**) and pure NiO (**b**) at the rate of 0.1 C, and cycling performances of pure NiO and NiO/MWCNT composites at the rate of 0.1 C (**c**) and at different current densities (**d**)

NiO/MWCNT composites at different cycles. In the first discharge process of the two anodes, a clear potential plateau at 0.85 V (vs. Li/Li^+) followed by a slope indicates the conversion reaction from NiO to Ni and the electrolyte decomposition. The charge plateau at 2.2 V corresponds to the NiO formation and Li_2O decomposition, while the peak at 1.6 V might attribute to the dissolution of SEI layer [24], respectively. This phenomenon is consistent with the other transition metal oxides such as Fe_2O_3, CuO, MnO, MnO_2, and CeO_2. The NiO shows a first discharge capacity of 982 mAh g^{-1}, which drops to 752 mAh g^{-1} in the 2nd cycle and quickly decreases to 49 mAh g^{-1} in the 50th cycle, showing a poor cycling performance. For the NiO/MWCNT composites, they show a higher initial discharge capacity of 1,015 mAh g^{-1} and the reversible charge capacity is 759 mAh g^{-1}. The corresponding irreversible capacity loss is 25 %, it may be mainly attributed to the formation of SEI film and the decomposition of electrolyte [25–29]. More importantly, the capacity remains at 868 mAh g^{-1} in the 50th cycle. Figure 5c displays the cycling performance of NiO and NiO/MWCNT composites. It can be clearly observed that the NiO/MWCNT composites exhibit remarkably excellent cycling stability. The enhanced cyclability of NiO/MWCNT composites should be attributed to the synergetic effects. First, the nanosized NiO can reduce the Li^+ diffusion distance and increase the contact area between the electrode material and the electrolyte. It also will release the volume expansion effectively. Second, MWCNTs as a buffering matrix can release the volume expansion and suppress the aggregation of active particles during the lithiation/delithiation process. Additionally, MWCNTs can effectively increase the electrical conductivity of the composite. The reversible capacity of the composites gradually increases from the 7th cycle and this phenomenon is consistent with the previous report [30, 31].The increasing capacity may be ascribed to the growth of the gel-like polymeric layer and possibly electrochemical activation of the hybrid composites during the cycling process [32–34]. Figure 5d shows the cycling performances of both NiO/MWCNT composites and pure NiO at various current densities. The NiO/MWCNT composites show relatively better rate capability. And when the current density changed from 2 to 0.1 C, the specific capacity recovered again. But the rate performance of NiO/MWCNT composites is not satisfied at 1 C rate or higher, which may be because of the

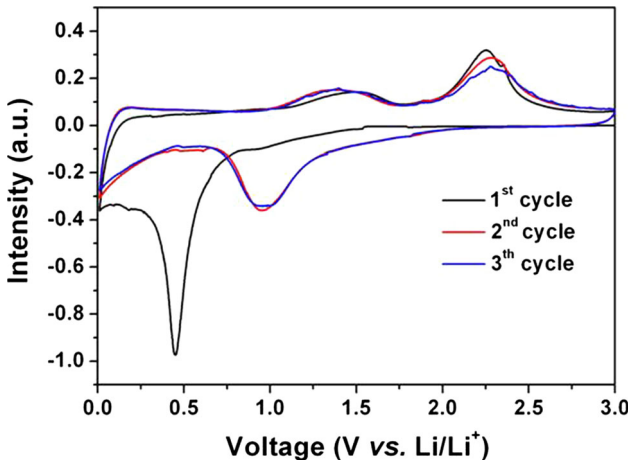

Fig. 6 The first three CV curves of NiO/MWCNT composites in the potential range of 0.01–3.0 V at a scan rate of 0.1 mV s^{-1}

uniformity of NiO on the MWCNTs or the relatively poor electrical conductivity of Li_2O generated during the discharge process. So experiments should be performed further to enhance the rate performance.

3.6 Cyclic voltammogram of NiO/MWCNT composites

The cyclic voltammogram (CV) curves of NiO/MWCNT composites at a scan rate of 0.1 mV s^{-1} in the potential range of 0.01–3.0 V are shown in Fig. 6. The profiles of CV curves for the 2nd and 3rd cycle are similar, whereas an obvious difference between the first and subsequent two cycles is found. During the first reduction scan, there is a strong reduction peak around 0.45 V, which is related to the initial reduction of NiO to Ni and formation of Li_2O, associating with the formation of a partially reversible solid electrolyte interface (SEI) [35]. The first anodic peaks at around 1.5 and 2.25 V correspond to the partial decomposition of the SEI layer and the formation of NiO, respectively [24, 36]. After the 1st cycle, the cathodic peak shifts to more positive potential and its intensity decreases significantly. The CV peaks show very good reproducibility after the first scan cycle.

4 Conclusions

In this study, NiO/MWCTN composites were successfully synthesized via a vacuum solution infiltration method and a subsequent calcination treatment at 350 °C for 2 h. SEM and TEM images show that the NiO particles are homogeneously distributed on the MWCNTs with a diameter of about 12 nm. The NiO/MWCNT composites electrode delivers a high reversible capacity of 873 mAh g^{-1} at a current density of 0.1 C at the 50th cycle, which maintains 86 % of the initial capacity. This high performance is ascribed to the MWCNTs which act as a buffering matrix and electron conductors in the composite; meanwhile, the nanosized NiO with faster Li^+ diffusion coefficient can also release the volume expansion effectively.

Acknowledgments This work was supported by Major Science and Technology Projects in Henan Province (121100210500).

References

1. Xia Y, Xiao Z, Dou X, Huang H, Lu X, Yan R, Gan Y, Zhu W, Tu J, Zhang W (2013) Green and facile fabrication of hollow porous MnO/C microspheres from microalgaes for lithium-ion batteries. ACS Nano 7:7083–7092
2. Liu Y, Wang DP, Yu YX, Zhang WD (2012) Preparation and photoelectrochemical properties of functional carbon nanotubes and Ti co-doped Fe_2O_3 thin films. Int J Hydrogen Energy 37:9566–9575
3. Mo Y, Ru Q, Song X, Hu S, An B (2014) A novel dendritic crystal Co_3O_4 as high-performance anode materials for lithium-ion batteries. J Appl Electrochem 44:781–788
4. Abbas SM, Hussain ST, Ali S, Abbas F, Ahmad N, Ali N, Khan Y (2013) One-pot synthesis of a composite of monodispersed CuO nanospheres on carbon nanotubes as anode material for lithium-ion batteries. J Alloys Compd 574:221–226
5. Chaudhari S, Srinivasan M (2012) 1D hollow α-Fe_2O_3 electrospun nanofibers as high performance anode material for lithium ion batteries. J Mater Chem 22:23049
6. Ding YL, Wu CY, Yu HM, Xie J, Cao GS, Zhu TJ, Zhao XB, Zeng YW (2011) Coaxial MnO/C nanotubes as anodes for lithium-ion batteries. Electrochim Acta 56:5844–5848
7. Zhao G, Zhang L, Pan T, Sun K (2013) Preparation of NiO/multiwalled carbon nanotube nanocomposite for use as the oxygen cathode catalyst in rechargeable Li–O_2 batteries. J Solid State Electrochem 17:1759–1764
8. Zhang G, Chen Y, Qu B, Hu L, Mei L, Lei D, Li Q, Chen L, Li Q, Wang T (2012) Synthesis of mesoporous NiO nanospheres as anode materials for lithium ion batteries. Electrochim Acta 80:140–147
9. Aravindan V, Suresh KP, Sundaramurthy J, Ling WC, Ramakrishna S, Madhavi S (2013) Electrospun NiO nanofibers as high performance anode material for Li-ion batteries. J Power Sources 227:284–290
10. Zou Y, Wang Y (2011) NiO nanosheets grown on graphene nanosheets as superior anode materials for Li-ion batteries. Nanoscale 3:2615–2620
11. Liu X, Or SW, Jin C, Lv Y, Feng C, Sun Y (2013) NiO/C nanocapsules with onion-like carbon shell as anode material for lithium ion batteries. Carbon 60:215–220
12. Qiu D, Xu Z, Zheng M, Zhao B, Pan L, Pu L, Shi Y (2012) Graphene anchored with mesoporous NiO nanoplates as anode material for lithium-ion batteries. J Solid State Electrochem 16:1889–1892
13. Shin DH, Lee JS, Jun J, Jang J (2014) Fabrication of amorphous carbon-coated NiO nanofibers for electrochemical capacitor applications. J Mater Chem A 2:3364
14. Mai YJ, Shi SJ, Zhang D, Lu Y, Gu CD, Tu JP (2012) NiO-graphene hybrid as an anode material for lithium ion batteries. J Power Sources 204:155–161
15. Dung NQ, Patil D, Jung H, Kim J, Kim D (2013) NiO-decorated single-walled carbon nanotubes for high-performance nonenzymatic glucose sensing. Sensor Actuat B Chem 183:381–387

16. Mustansar AS, Tajammul HS, Ali S, Shahzad MK, Ahmad N, Ali N (2013) Facile synthesis of carbon nanotubes supported NiO nanocomposite and its high performance as lithium-ion battery anode. Mater Lett 107:158–161
17. Xu C, Sun J, Gao L (2011) Large scale synthesis of nickel oxide/multiwalled carbon nanotube composites by direct thermal decomposition and their lithium storage properties. J Power Sources 196:5138–5142
18. Ding C, Lin H, Sato K, Hashida T (2009) Synthesis of NiO-$Ce_{0.9}Gd_{0.1}O_{1.95}$ nanocomposite powders for low-temperature solid oxide fuel cell anodes by co-precipitation. Scripta Mater 60:254–256
19. Wen B, Zhang S, Fang H, Liu W, Du Z (2011) Electrochemically dispersed nickel oxide nanoparticles on multi-walled carbon nanotubes. Mater Chem Phys 131:8–11
20. Lu H-W, Li D, Sun K, Li YS, Fu ZW (2009) Carbon nanotube reinforced NiO fibers for rechargeable lithium batteries. Solid State Sci 11:982–987
21. Hu R, Sun W, Liu H, Zeng M, Zhu M (2013) The fast filling of nano-SnO_2 in CNTs by vacuum absorption: a new approach to realize cyclic durable anodes for lithium ion batteries. Nanoscale 5:11971–11979
22. Xia H, Lai M, Lu L (2010) Nanoflaky MnO_2/carbon nanotube nanocomposites as anode materials for lithium-ion batteries. J Mater Chem 20:6896
23. Wang C, Wang D, Wang Q, Chen H (2010) Fabrication and lithium storage performance of three-dimensional porous NiO as anode for lithium-ion battery. J Power Sources 195:7432–7437
24. Susantyoko RA, Wang X, Xiao Q, Fitzgerald E, Zhang Q (2014) Sputtered nickel oxide on vertically-aligned multiwall carbon nanotube arrays for lithium-ion batteries. Carbon 68:619–627
25. Jang B, Park M, Chae OB, Park S, Kim Y, Oh SM, Piao Y, Hyeon T (2012) Direct synthesis of self-assembled ferrite/carbon hybrid nanosheets for high performance lithium-ion battery anodes. J Am Chem Soc 134:15010–15015
26. Rai AK, Anh LT, Gim J, Mathew V, Kang J, Paul BJ, Singh NK, Song J, Kim J (2013) Facile approach to synthesize CuO/reduced graphene oxide nanocomposite as anode materials for lithium-ion battery. J Power Sources 244:435–441
27. Chen WM, Qie L, Shen Y, Sun YM, Yuan LX, Hu XL, Zhang WX, Huang YH (2013) Superior lithium storage performance in nanoscaled MnO promoted by N-doped carbon webs. Nano Energy 2:412–418
28. Li X, Chun XC, Chun HM (2011) Facile synthesis of α/MnO_2-graphene nanocomposites and their high performance as lithium-ion battery anode. Mater Lett 65:2104–2106
29. Wang G, Bai J, Wang Y, Ren Z, Bai J (2011) Prepartion and electrochemical performance of a cerium oxide–graphene nanocomposite as the anode material of a lithium ion battery. Scripta Mater 65:339–342
30. Kumar RA, Tuan AL, Park CJ, Kim J (2013) Electrochemical study of NiO nanoparticles electrode for application in rechargeable lithium-ion batteries. Ceram Int 39:6611–6618
31. Mao Y, Kong Q, Guo B, Shen L, Wang Z, Chen L (2013) Polypyrrole-NiO composite as high-performance lithium storage material. Electrochim Acta 105:162–169
32. Xu X, Dong B, Ding S, Xiao C, Yu D (2014) Hierarchical Ni-CoO_2 nanosheets supported on amorphous carbon nanotubes for high-capacity lithium-ion batteries with a long cycle life. J Mater Chem A 2:13069
33. Jiang Y, Zhang D, Li Y, Yuan T, Bahlawane N, Liang C, Sun W, Lu Y, Yan M (2014) Amorphous Fe_2O_3 as a high-capacity, high-rate and long-life anode material for lithium ion batteries. Nano Energy 4:23–30
34. Xu X, Fan Z, Yu X, Ding S, Yu D, Lou XWD (2014) A Nanosheets-on-channel architecture constructed from MoS_2 and CMK-3 for high-capacity and long-cycle-life lithium storage. Adv Energy Mater. doi:10.1002/aemn.201400902
35. Chen Z, Xiao A, Chen Y, Zuo C, Zhou S, Li L (2012) Template-directed preparation of two-layer porous NiO film via hydrothermal synthesis for lithium ion batteries. Mater Res Bull 47:1987–1990
36. Wang H, Pan Q, Wang X, Yin G, Zhao J (2009) Improving electrochemical performance of NiO films by electrode position on foam nickel substrates. J Appl Electrochem 39:1597–1602